Journal of the European Ceramic Society 41 (2021) 4850–4858

Contents lists available at ScienceDirect

Journal of the European Ceramic Society

journal homepage: www.elsevier.com/locate/jeurceramsoc

Multiscale phase homogeneity in bulk nanocrystalline high entropy oxides

Alexander D. Dupuy [a,*], Mohammed Reda Chellali [b], Horst Hahn [a,b,c], Julie M. Schoenung [a]

[a] Department of Materials Science and Engineering, University of California, Irvine, USA
[b] Institute of Nanotechnology, Karlsruhe Institute of Technology, 76344, Eggenstein-Leopoldshafen, Germany
[c] KIT-TUD Joint Research Laboratory Nanomaterials, Institute of Materials Science, Technical University Darmstadt, 64206, Darmstadt, Germany

ARTICLE INFO

Keywords:
High entropy oxide (HEO)
Nanocrystallinity
Phase homogeneity
Atom probe tomography (APT)
Spark plasma sintering (SPS)

ABSTRACT

X-ray diffraction, energy dispersive X-ray spectroscopy, and atom probe tomography (APT) were used to assess the phase homogeneity of bulk sintered (Cu, Co, Mg, Ni, Zn)O transition metal high entropy oxides (TM-HEOs) across multiple length scales. These three methods were applied to both coarse-grain and nanocrystalline TM-HEO samples sintered using two different processing routes. Coarse-grain samples were prepared by reaction sintering of unreacted nanopowders using conventional sintering, while nanocrystalline samples were prepared from solid-state synthesized nanopowders consolidated using spark plasma sintering. Despite the different processing methods and grain sizes, the TM-HEO samples exhibit little-to-no chemical or phase segregation across all length scales. Critically, APT confirms that there is no chemical segregation at the nm scale even after solid-state synthesis and high temperature consolidation.

1. Introduction

High entropy stabilization has emerged as a powerful method for achieving single-phase solid solution structures in chemically complex materials. Such materials have five or more components and make use of a high entropy to achieve a single-phase state. The high entropy design concept was first applied to oxide materials in the form of high entropy oxides (HEO) with the (Cu, Co, Mg, Ni, Zn)O transition metal HEO (TM-HEO) system [1]. At high temperatures (>850 °C), a random solid solution rocksalt crystal structure is stable in TM-HEO due to the metal cations randomly populating their sublattice, leading to an entropy that is large enough to outcompete other enthalpy-driven configurations. Limited solubility among the constituent oxides is one source of enthalpy-driven configurations. In TM-HEO, two of the constituent oxides, ZnO and CuO, are not rocksalt under ambient conditions, resulting in limited solubility in the rocksalt crystal structure. Critically, high entropy enables TM-HEOs to be phase-pure after appropriate processing, despite their chemical complexity. TM-HEO has been studied extensively and shows promise in applications such as capacitors [2], catalysts [3], and solid state electrolytes [4]. Additional HEO systems have also been explored and found to form single phase solid solution structures, such as multi-cationic perovskites [5] and multi-anionic oxy-fluorites [6]. It is thought that the high entropy confers a stabilizing effect in HEOs, allowing for improved cycling stability in energy storage systems [7] and high temperature stability in catalyst systems [3].

Poor solubility among some of the constituent oxides can lead to an inhomogenous multi-phase structure after processing due to two reasons: an incomplete solid-state reaction between the components and the segregation of enthalpy-driven secondary phases. Incorporating five or more oxide components in equiatomic amounts often requires a complicated reaction sequence, especially if one or more components violate Hume-Rothery rules and have poor solubility in the solid solution structure. Hong et al. found that TM-HEO is formed in a complex solid-state reaction process, with each binary oxide component in the MgO-CoO-NiO-CuO-ZnO system dissolving into the rocksalt solid-solution structure at different temperatures [8]. An insufficient reaction temperature will yield samples with inhomogeneities associated with the unreacted constituents, potentially resulting in inferior properties compared to a fully reacted sample. The complexity involved in forming single-phase HEO materials necessitates careful evaluation of the phase homogeneity after processing.

Additionally, TM-HEOs easily transform between an entropy-driven metastable single-phase state and an enthalpy-driven equilibrium multi-phase state. While the single-phase state consists of the rocksalt crystal structure, the multi-phase state contains both a rocksalt phase and a secondary tenorite phase. TM-HEO displays a temperature window of ~650−850 °C where this secondary phase forms. Heat treatment within this temperature window results in varying levels of phase

* Corresponding author.
E-mail address: dupuya@uci.edu (A.D. Dupuy).

https://doi.org/10.1016/j.jeurceramsoc.2021.03.035
Received 25 January 2021; Received in revised form 16 March 2021; Accepted 18 March 2021
Available online 20 March 2021

heterogeneity. We refer to this temperature window and the resulting phase heterogeneity as the *phase spectrum* [9]. Conversely, heat treatment at temperatures >850 °C are necessary to yield the single-phase state. In our previous work, we used X-ray diffraction (XRD) to investigate the phase homogeneity in bulk sintered TM-HEO, finding that bulk samples prepared using reaction sintering or sintering of solid-state synthesized nanopowders exhibit phase homogeneity at the macroscale when heat treated above 850 °C [9]. In another study, we used atom probe tomography (APT) to demonstrate that single-phase TM-HEO nanopowders synthesized with nebulized spray pyrolysis exhibit phase homogeneity at the nm scale [10]. But the extent of the phase homogeneity at the nm scale has not yet been evaluated for the single-phase, bulk sintered material, the importance of which is described below.

Our previous studies have revealed that the secondary phase in bulk sintered TM-HEO is a Cu-rich multicomponent phase [9] and that the phase transformation is strongly influenced by grain size, with smaller grain sizes changing the amount of secondary phase and the temperature range at which the secondary phase forms. Further, the Cu-rich phase manifests as needle and particle-shaped morphologies in coarse-grain samples and as individual Cu-rich grains in nanocrystalline samples. Heat treating the consolidated TM-HEO above the entropic transformation temperature (>850 °C) results in a single-phase state containing only the rocksalt crystal structure, as determined by XRD, regardless of grain size. However, due to the chemical complexity and capability of forming secondary phases, consolidated single-phase bulk TM-HEO could have local chemical or phase segregation at the nm scale that cannot be detected using XRD or SEM. APT is an effective method of analyzing the chemical distribution of a three-dimensional volume at the nm scale, allowing for the visualization of local segregation [11]. Our APT characterization of TM-HEO single-phase nanopowders synthesized using nebulized spray pyrolysis revealed no chemical segregation at the nm scale, which we attributed to the high temperatures (1150−1250 °C) and short residence times (<1 s) used during synthesis [10]. APT confirmed that these nanopowders exhibited no signs of secondary phase formation nor clustering of atoms, indicating that TM-HEO nanopowders can achieve full phase homogeneity.

Ultimately though, TM-HEO materials need to be made in bulk form if they are to be used in many of the applications currently being explored. The previously discussed single-phase TM-HEO nanopowders were not exposed to the thermal conditions required to sinter bulk samples [10]. Yet sintering can unintentionally introduce or retain phase heterogeneities that can significantly impact properties [12]. Additionally, phase segregation in HEO materials will cause the stoichiometry of the entropy-driven phase to deviate from equimolarity, reducing the entropy and potentially jeopardizing the stability of the material. While a significant amount of work has been done on understanding the properties of HEO materials [13,14], comparatively little work has been done on understanding their complex reaction, sintering, and phase segregation behavior. It is therefore important to study the phase homogeneity in TM-HEO after sintering to form a consolidated bulk material, especially given the complex reaction process and known propensity for phase segregation at intermediate temperatures. Thus, the purpose of this study is to explore the phase homogeneity in bulk consolidated TM-HEO at the nm scale through the application of APT; XRD and SEM are also used to confirm macro-scale phase homogeneity. Variable sintering approaches and as-sintered grain size values are evaluated to explore the robustness of the findings.

2. Experimental methods

2.1. Solid-state powder synthesis

TM-HEO nanopowders were prepared using solid-state synthesis methods. Oxide nanopowders (US Research Nanomaterials Inc, Houston, TX, USA) of CuO (25−55 nm reported particle size, 99.95 wt% purity), CoO (50 nm, 99.7 %), MgO (50 nm, 99.95 %), NiO (18 nm, 99.98 %), and ZnO (18 nm, 99.95 %) were blended using a mortar and pestle in equimolar amounts. Further blending was performed using a Fritsch Premium 7 (Fritsch GmbH, Idar-oberstein, Germany) planetary ball mill (PBM) at 300 rpm for 3 h. Powders were suspended in isopropanol and milled using Si_3N_4 jars and media. These unreacted nanopowder mixtures are hereafter referred to as *blended oxide nanopowders*. Some of the blended oxide nanopowders were heat treated at 900 °C for 20 min to form a coarse-grain single-phase TM-HEO powder. These powders were reground in the PBM at 300 rpm for 12 h and are hereafter referred to as *pre-reacted nanopowders*.

2.2. Bulk sample consolidation

Conventional sintering and spark plasma sintering (SPS) were used to consolidate the blended oxide and pre-reacted nanopowders into bulk TM-HEO samples. Conventional sintering was performed using an elevator furnace (Model 1210BL, CM Furnaces, Bloomfield, NJ, USA) at a temperature of 1100 °C for 12 h in order to consolidate the blended oxide nanopowders into bulk coarse-grain samples. The samples were quenched to room temperature by lowering the furnace elevator into the path of a fan blowing room temperature air. A Fuji model 825S SPS instrument (Fuji Electronic Industrial Co., Ltd., Kawasaki, Japan) was used to consolidate the blended oxide and pre-reacted nanopowders into bulk nanocrystalline samples. SPS was performed at a temperature of 700 °C for 5 min with a heating rate of 200 °C/min. An applied pressure of 100 MPa was used throughout the experiment.

2.3. Phase and microstructural characterization

The density of the bulk samples was measured using Archimedes method, and the relative density was calculated based on a theoretical density of 6.137 g/cm^3 [15]. A Regulus 8230 SEM (Hitachi, Tokyo, Japan) was used to examine the microstructure of the bulk samples and powders. Average grain sizes were found by examining fractured specimen surfaces. Chemical mapping was performed on flat polished samples using a QUANTAX FlatQUAD (Bruker, Billerica, MA, USA) energy dispersive X-ray spectroscopy (EDS) instrument. Maps were acquired using an accelerating voltage of 3 kV in order to achieve the spatial resolutions necessary to observe small (<100 nm) inhomogeneities that might be present in the samples. The maps were analyzed and prepared using the Bruker ESPRIT software. It is important to note that the color intensity of the maps presented in this work are relative, and do not represent a quantified composition. An Ultima III XRD instrument (Rigaku, Tokyo, Japan) was used to analyze the phase state of the samples.

2.4. Atom probe tomography

APT samples were prepared using an Auriga 60 (Zeiss, Oberkochen, Germany) focused ion beam (FIB) system. A platinum capping layer (150 nm in thickness) was deposited over the area of interest to protect from Ga ion damage during milling. To produce the required atom probe specimen geometry, annular milling was used to create needle-shaped specimens with a tip diameter of <100 nm [16]. APT measurements were performed using a LEAP 4000X HR (Cameca SAS, Gennevilliers, Cedex, France) in laser pulse mode (pulse energy 60 pJ, pulse frequency 100 kHz) at 50 K. Cameca's integrated visualization and analysis software (IVAS) was used for reconstruction analysis. Depth profiles were calculated using a 6 nm diameter cylinder along the long axis of the needle.

Statistical analysis of APT data is a powerful method of analyzing subtle variations in local chemistry that are not detectible from simple visual analysis of the measured APT volumes. In this work, the extent of chemical clustering was assessed using nearest neighbor (NN) and frequency distribution analysis. Both of these techniques have been used extensively to extract information about chemical clustering from APT

data of high entropy materials [17,10]. In this work, the first (1NN) and fifth (5NN) nearest neighbor distributions were calculated and compared to a random label swapped data set. Significant chemical clustering is likely to exist when the NN distributions display multi-modal behavior or significantly deviate from the randomized data set. Frequency distribution analysis was used to calculate Pearson coefficients for the five binary oxide constituents in TM-HEO. Pearson coefficients measured from APT data sets can be used to quantitatively measure the extent of clustering [18]. Pearson coefficients range from 0 to 1, with 1 corresponding to complete separation of the element or compound, and 0 corresponding to a random binomial distribution.

3. Results and discussion

3.1. Microstructure and phase state

Nanopowders synthesized using the blended oxide method display XRD peaks from the constituent binary oxides, confirming that blended oxide nanopowders are an unreacted mixture of the five starting nanopowders (Fig. 1a–i). XRD peaks corresponding to the constituent oxide nanopowders are labeled as: 'Z' for ZnO, 'C' for CuO, 'M' for MgO, and 'N' for NiO in Fig. 1a. Distinct CoO peaks are not observed due to overlap with the peaks of the other constituent oxides. As a mixture of the unreacted binary nanopowders, blended oxide nanopowders contain primarily individual and agglomerated nanoparticles with features similar in size to the reported particle sizes of the individual binary oxide nanopowders (≤55 nm), as seen in the SEM micrograph in Fig. 1b. XRD reveals that blended oxide nanopowders consolidated with conventional sintering have a single-phase rocksalt crystal structure with no signs of extraneous peaks (Fig. 1a–ii). The conventionally sintered samples have a coarse-grain equiaxed microstructure with an average grain size of 15 μm (Fig. 1c), and an as-consolidated relative density of 99 %. The high temperatures (1100 °C) and long hold times (12 h) involved in our conventional sintering process result in the reaction of the blended oxide nanopowders into the single-phase TM-HEO crystal structure and the considerable grain growth that we observe. We hereafter refer to these single-phase bulk samples as the *single-phase coarse-grain samples*.

SPS processing of blended oxide nanopowders yields bulk TM-HEO samples with multiple phases, displaying XRD peaks corresponding to the TM-HEO rocksalt phase, as well as extraneous peaks corresponding to the unreacted CuO and ZnO constituent oxide nanopowders (Fig. 1a–iii). Although CoO peaks are not directly observed, peaks corresponding to Co_3O_4 or a Co-rich spinel phase can be identified (labeled as 'S' in Fig. 1a). The presence of peaks from the starting powders indicates that the solid-state reaction into a single-phase TM-HEO rocksalt crystal structure has not yet come to completion in these samples. These unreacted SPS consolidated samples display a nanocrystalline microstructure with an average grain size of 81 nm, as seen in Fig. 1d. We refer to these unreacted bulk samples here as *unreacted nanocrystalline samples*.

The unreacted nanocrystalline samples retain the nanocrystalline microstructure and morphology of the blended oxide nanopowders due to the low temperatures and short processing times involved in our SPS processing. Furthermore, the SPS processing conditions used in this study are insufficient to fully react the blended oxide nanopowders during sintering, yielding a multi-phase state. Our previous work has shown that temperatures >800 °C are necessary to complete the in-situ solid-state reaction and achieve a single-phase rocksalt crystal structure [9]. Such high temperatures will yield significant grain growth and are incompatible with retaining a nanocrystalline microstructure in TM-HEO.

In order to produce bulk nanocrystalline TM-HEO samples with a single-phase rocksalt crystal structure, it is necessary to complete the solid-state reaction before consolidation using SPS. We have previously shown that heat treating blended oxide nanopowders at 900 °C for 20 min is sufficient to form single-phase TM-HEO powders [9]. PBM of those heat-treated powders results in single-phase nanopowders with XRD patterns showing only broad rocksalt peaks (Fig. 2a). These pre-reacted nanopowders display individual and agglomerated nanoparticles after PBM, as seen in Fig. 2b. These results confirm that single-phase TM-HEO nanopowders can be synthesized from solid-state reaction and PBM [9]. SPS consolidation of pre-reacted nanopowders at 700 °C yields bulk samples with a predominantly single-phase rocksalt crystal structure. Although small peaks corresponding to the Cu-rich tenorite phase (denoted with 'T' in Fig. 2a) can be observed, Rietveld refinement using MAUD [19] indicates that the tenorite phase content is <1 at%. Thus, we consider these as-consolidated samples to be essentially 'single' phase. These SPS-consolidated samples have nanocrystalline microstructures with an average grain size of 97 nm (Fig. 2c), and as such, we refer to them here as *single-phase nanocrystalline samples*. The

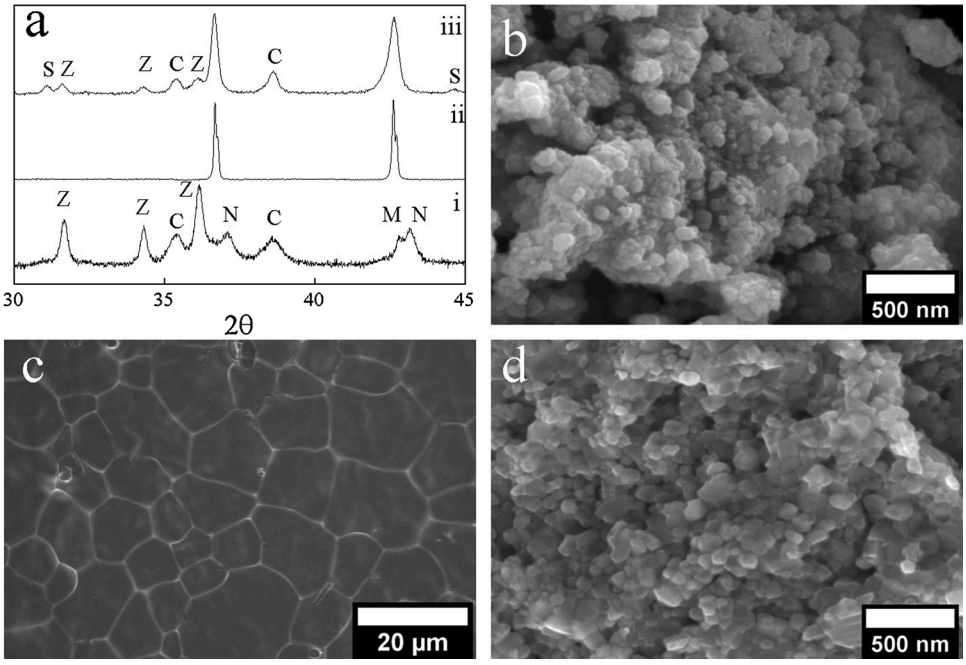

Fig. 1. Synthesis and consolidation of bulk TM-HEO ceramics from blended oxide nanopowders. (a) X-ray diffraction patterns for: (i) the blended oxide nanopowder and the samples consolidated from the blended oxide nanopowder using: (ii) conventional sintering (single-phase coarse-grain samples) and (iii) spark plasma sintering (unreacted nanocrystalline samples). Peaks corresponding to additional phases and the constituent oxide nanopowders are labeled as: 'S' for the Co-rich spinel phase, 'Z' for ZnO, 'C' for CuO, 'M' for MgO, and 'N' for NiO; (b) micrograph of the blended oxide nanopowders; (c) fracture surface micrograph of a single-phase coarse-grain sample; and (d) fracture surface micrograph of an unreacted nanocrystalline sample.

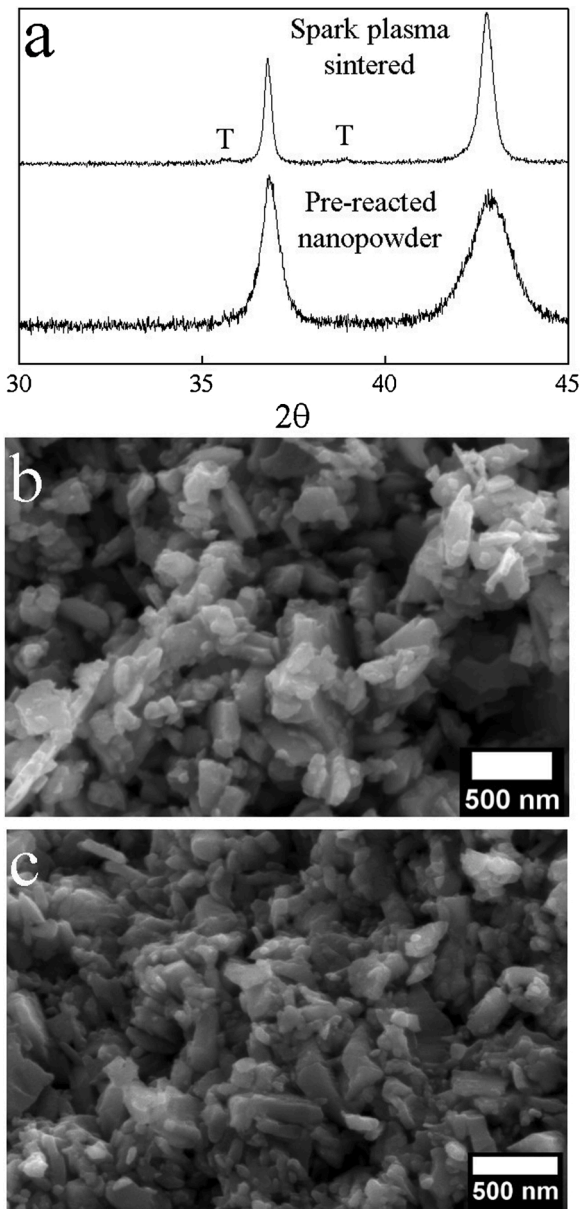

Fig. 2. Synthesis and consolidation of bulk TM-HEO ceramics from pre-reacted nanopowders. (a) X-ray diffraction patterns for the pre-reacted nanopowder and spark plasma sintered single-phase nanocrystalline samples. Peaks corresponding to the Cu-rich tenorite phase are labeled as 'T'; (b) micrograph of the pre-reacted nanopowders; and (c) fracture surface micrograph of a sintered single-phase nanocrystalline sample.

low temperature (700 °C) and short hold time (5 min) involved in SPS consolidation enable the retention of the nanocrystalline microstructure present in the pre-reacted nanopowders. Despite being sintered at the maximum tenorite formation temperature (700 °C), the short processing time allows for the creation of samples with minimal amounts of secondary phase [9]. The single-phase nanocrystalline samples have relative densities of >98 %.

3.2. Macro-scale phase homogeneity

Our previous work demonstrates that low voltage EDS (3 kV accelerating voltage) is an effective method for visualizing the small (~100 nm) secondary phases in multi-phase TM-HEO [9]. Using these same EDS measurement conditions reveals no sign of the Cu-rich phase in the single-phase coarse-grain samples made from blended oxide nanopowders (Fig. 3). Segregation of the other elements is also not observed. Thus, in the single-phase coarse-grain samples, the high-temperature conventional sintering procedure is sufficient to fully react the blended oxide nanopowders and achieve macroscopic phase homogeneity.

In the unreacted nanocrystalline samples, significant inhomogeneity is observed, as seen from the chemical maps in Fig. 4. The inhomogeneities visible in the EDS maps are similar in size to the individual or agglomerated nanoparticle morphologies found in the blended oxide nanopowders (Fig. 1b). XRD patterns of these samples contain extraneous peaks corresponding to the starting powders (Fig. 1a), implying that these inhomogeneous regions are the unreacted constituent oxide nanopowders. As previously described by Hong et al., the solid-state reaction involved in reacting the MgO-CoO-NiO-CuO-ZnO system into single-phase rocksalt TM-HEO is complex [8]. The five binary oxide components have varying levels of solubility in the rocksalt crystal structure and will dissolve into the solid solution structure at different temperatures. Hong et al., relate the order that the binary oxide components dissolve to their vacancy formation energy. Of the rocksalt binary oxides, MgO (1.8−2 eV [20]) and CoO (1.83 eV [21]) have the lowest vacancy formation energy and are expected to react first, while NiO (4.35 eV [22]) has a greater vacancy formation energy and would be expected to react after MgO and CoO. CuO and ZnO do not stabilize in a rocksalt crystal structure under ambient conditions and are observed dissolving into the rocksalt structure last.

Based on the vacancy formation energies and the observations of Hong et al. [8], the binary oxides would be expected to dissolve in the following order: (1) MgO and CoO, (2) NiO, (3) ZnO, (4) CuO. However, in our unreacted nanocrystalline samples the Ni EDS map displays the least amount of inhomogeneity out of all five metal element EDS maps. MgO and CoO would be expected to react before NiO due to their lower vacancy formation energies. We attribute the lack of Ni inhomogeneities to the NiO nanopowder having an 18 nm reported particle size, which is smaller than the 50 nm reported particle sizes of the MgO and CoO nanopowders. A smaller particle size will allow the NiO nanopowder to dissolve more readily into the TM-HEO rocksalt crystal structure.

In addition to CuO and ZnO peaks, the XRD pattern of the unreacted nanocrystalline samples also displays peaks corresponding to Co_3O_4 spinel or a Co-rich spinel phase of the form MCo_2O_4 (where M=Cu, Mg, Ni, Zn). Upon close examination of the cation EDS maps, significant overlap is not observed between the signals in the Co map and the maps for the four other metals. In other words, there is mostly an absence of signal in the Cu, Ni, Mg, and Zn EDS maps in the locations where the Co-rich particles reside. Although it is difficult to pinpoint the composition of the spinel phase in the unreacted nanocrystalline samples, our EDS results indicate that the Co-rich particles are likely to be Co_3O_4. CoO is known to transform to Co_3O_4 between 600−900 °C [23], with smaller particles sizes decreasing the transformation temperature [24]. However, CoO is able to form spinel phases with the other metals in TM-HEO [25]. Additionally, some Co-rich regions overlap with Zn signals, indicating a possible reaction between CoO and ZnO to form $ZnCo_2O_4$. We therefore propose that CoO goes through an intermediate transformation and reaction step to Co_3O_4 or $ZnCo_2O_4$ before finally dissolving into the TM-HEO rocksalt crystal structure.

The XRD pattern for the unreacted nanocrystalline samples displays peaks corresponding to the TM-HEO rocksalt crystal structure as well as unreacted CuO, ZnO, and a Co-rich spinel phase (Fig. 1a). Peaks corresponding to unreacted MgO and NiO are not observed. However, the EDS maps for the unreacted samples indicate that none of the five binary oxides have completely dissolved into the rocksalt crystal structure, including MgO and NiO. The disparity between the measurements can be attributed to the amount of unreacted MgO and NiO being below the detection limit of XRD. Given the complexity of the solid-state reaction process in HEO materials, such an observation illustrates that XRD alone may not be sufficient for determining phase homogeneity. Multiple measurement techniques are necessary to thoroughly investigate the

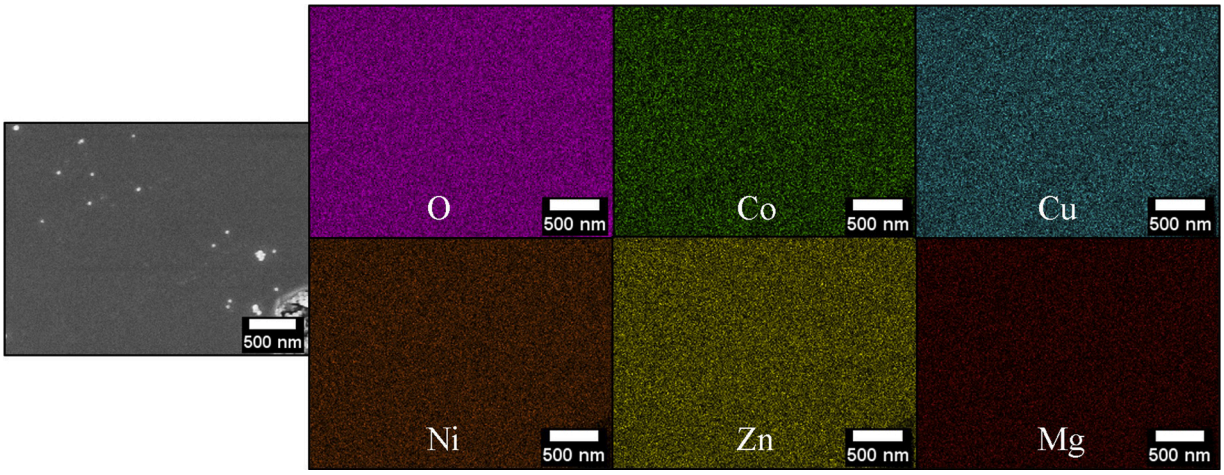

Fig. 3. Phase and chemical homogeneity of the single-phase coarse-grain samples: scanning electron micrograph and corresponding EDS chemical maps of a single-phase coarse-grain sample, which was consolidated from the blended oxide nanopowders using conventional sintering. Note that the bright features seen in the secondary electron micrograph (far left panel) are surface debris and a grain pullout. These features were used to help focus the microscope and are not related to the chemical behavior of the sample.

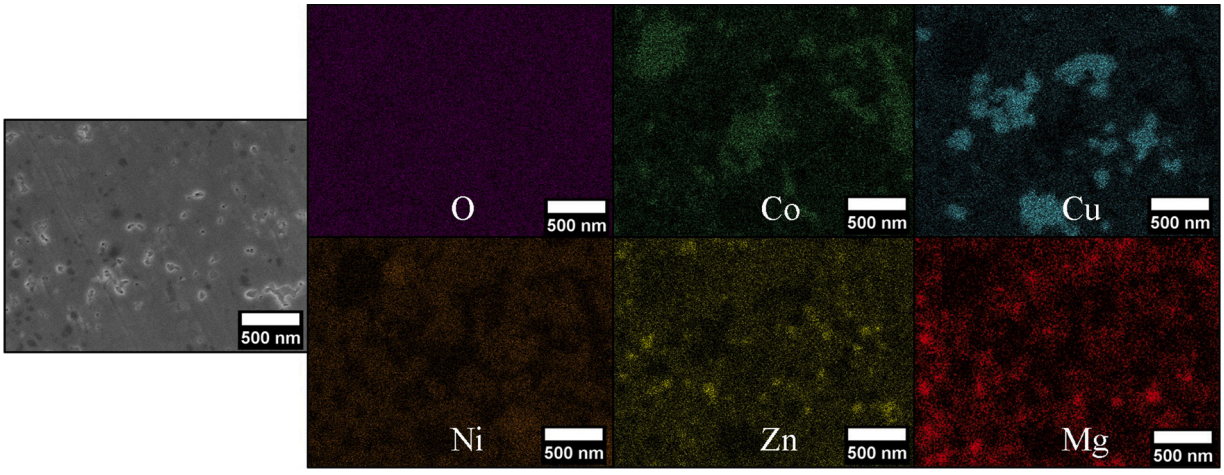

Fig. 4. Phase and chemical homogeneity of the unreacted nanocrystalline samples: scanning electron micrograph and corresponding EDS chemical maps of an unreacted nanocrystalline sample, which was consolidated from the blended oxide nanopowders using spark plasma sintering.

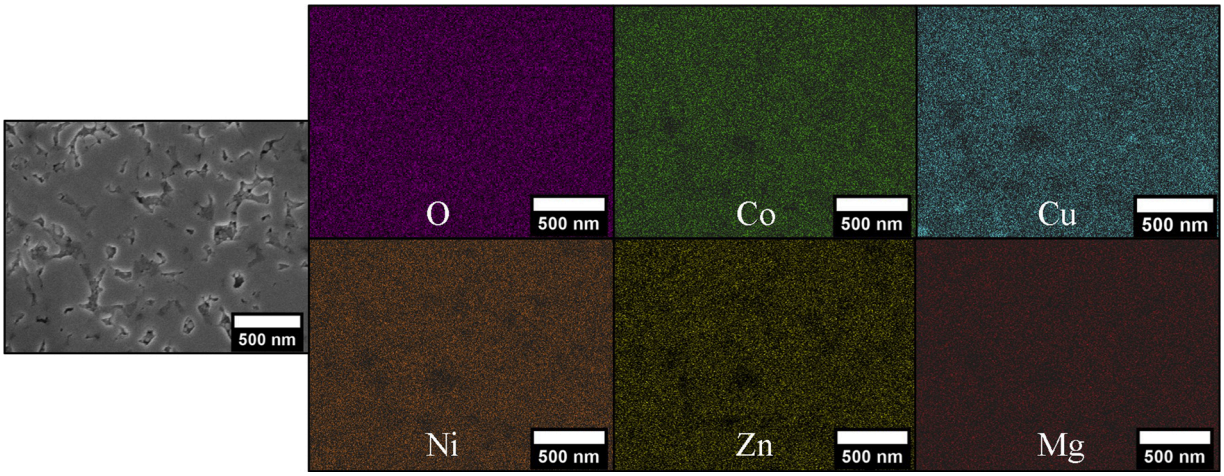

Fig. 5. Phase and chemical homogeneity of the single-phase nanocrystalline samples: scanning electron micrograph and corresponding EDS chemical maps of a single-phase nanocrystalline sample, which was consolidated from the pre-reacted nanopowders using spark plasma sintering.

phase homogeneity in HEO materials across a range of length scales.

In the single-phase nanocrystalline samples, occasional Cu-rich regions are observed in the EDS map (Fig. 5), which is consistent with our XRD data that indicate the presence of a minor amount of the Cu-rich phase. Additionally, no segregation is observed in the other EDS maps. It is important to draw a distinction between inhomogeneities from the unreacted constituent nanopowders and those which arise from secondary-phase segregation. In the unreacted nanocrystalline samples the inhomogeneous regions are of the same length scale as the agglomerates of the starting nanopowders. Conversely, the Cu-rich regions in the single-phase nanocrystalline samples are approximately the size and morphology of the nanocrystalline grains, which agrees with our previous observations that the segregated secondary phase generally encompasses an entire grain in nanocrystalline TM-HEO. Overall, however, in the single-phase nanocrystalline samples consolidated from pre-reacted nanopowders, little-to-no clustering of Cu is observed in the EDS maps indicating that these samples are 'single-phase' at this scale.

3.3. Nanometer-scale phase homogeneity

XRD and EDS reveal obvious signs of inhomogeneity in the unreacted nanocrystalline samples. Conversely, these same methods indicate that single-phase coarse-grain and nanocrystalline samples are single phase at the macroscopic scale. However, it is still possible for small secondary phases to be present in a sample that initially appears 'single-phase', due to an incomplete solid state reaction or TM-HEO's propensity to form secondary phases under certain conditions [9]. While XRD and SEM/EDS provide insight into the phase distribution across a wide range of length scales, these methods cannot provide information about the chemical distribution at the nm scale. In the present study, the phase homogeneity of the bulk sintered single-phase samples was evaluated using APT. The unreacted nanocrystalline samples were not considered for APT due to their inhomogeneity being indisputably verified using XRD and SEM.

A three-dimensional chemical reconstruction of all six elements in a single-phase coarse-grain sample can be observed in Fig. 6a. Color-coded dots represent individual atoms in the reconstruction. We observe that the single-phase coarse-grain sample displays no obvious signs of phase segregation throughout the volume. The phase homogeneity was examined qualitatively by performing a composition depth profile analysis along the length of the needle (Fig. 6b). No significant concentration fluctuations are observed in the sample.

The extent of clustering in the single-phase coarse-grain sample was more rigorously assessed using NN and binomial frequency distribution analysis. 1NN and 5NN distributions for CoO, CuO, MgO, NiO, and ZnO, along with the equivalent randomized distributions (dashed lines), can be seen in Fig. 7. None of the NN distributions display any bimodal nature for any of the oxides, indicating that there is no significant chemical clustering in the sample. Further, the NN distributions compare well to the randomized distributions. The Pearson coefficients, calculated from the binomial distribution of the individual binary oxides (not shown), can be seen in Table 1. The coefficients are all much less than 1, indicating no clustering of any of the oxides. Combined, the binomial distribution and the NN distribution analysis indicate that there is no significant chemical clustering in the single-phase coarse-grain samples at the nm scale.

It is important to note that our single-phase coarse-grain samples are prepared by reaction-sintering unreacted blended oxide nanopowders, which consist of five blended nanopowders. XRD and EDS results confirm that the coarse-grain samples are single phase down to 10's of nm, while APT confirms that the solid-state reaction is complete down to the nm scale. As discussed above, the blended oxide nanopowders have two constituent oxides (CuO and ZnO) that do not form into the rocksalt crystal structure under ambient conditions, resulting in a complex reaction sequence that involves the five components dissolving into the rocksalt solid solution crystal structure at different temperatures [8]. We show that phase homogeneity can be achieved in coarse-grain TM-HEO via solid-state reaction during conventional sintering, despite the complex reaction process. The phase homogeneity in our samples can be attributed to the temperature (1100 °C) and time (12 h) involved in conventional sintering, as well as the nanometric nature of the starting nanopowders (<50 nm particle size).

Our EDS results demonstrate that the single-phase nanocrystalline samples have the capability of forming minor amounts of secondary phase during consolidation (Fig. 5), suggesting that the primary rocksalt solid-solution phase may contain nm scale chemical segregation as well. A 3D atomic reconstruction of a single-phase nanocrystalline bulk TM-HEO sample can be seen in Fig. 8a. Like the single-phase coarse-grain samples, visible chemical clustering is not observed in the single-phase nanocrystalline samples. Composition depth profile analysis (Fig. 8b) displays no obvious concentration fluctuations.

Similar to the single-phase coarse-grain samples, the absence of chemical clustering in the single-phase nanocrystalline samples was further verified using NN and frequency distribution analysis. 1NN and 5NN distributions for the constituent binary oxides display no bimodal behavior and closely match the randomized distributions (Fig. 9). The Pearson coefficients calculated from the frequency distribution analysis of the oxides are also much less than 1 (Table 1). Taken together, these two analysis methods indicate the absence of significant chemical clustering at the nm scale in single-phase nanocrystalline samples. Inhomogeneities associated with an incomplete solid-state reaction would not be expected as our single-phase nanocrystalline samples were consolidated from single-phase pre-reacted nanopowders using SPS. Despite being sintered at 700 °C, at which secondary phases are known to form during heat treatment [9], our single-phase nanocrystalline samples show no signs of significant phase segregation. The rapid

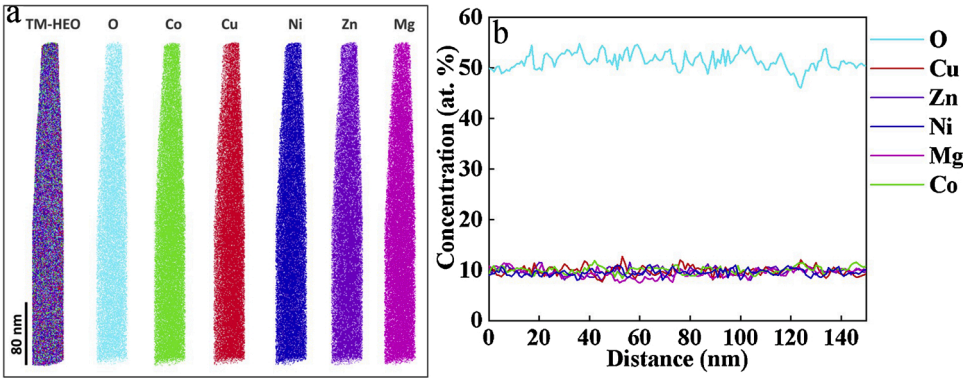

Fig. 6. Chemical distribution in a single-phase coarse-grain sample: (a) atom probe tomography (APT) 3D chemical distribution maps for a sintered single-phase coarse-grain sample; and (b) compositional profiles measured along a 6 nm diameter cylinder in the sintered single-phase coarse-grain APT sample.

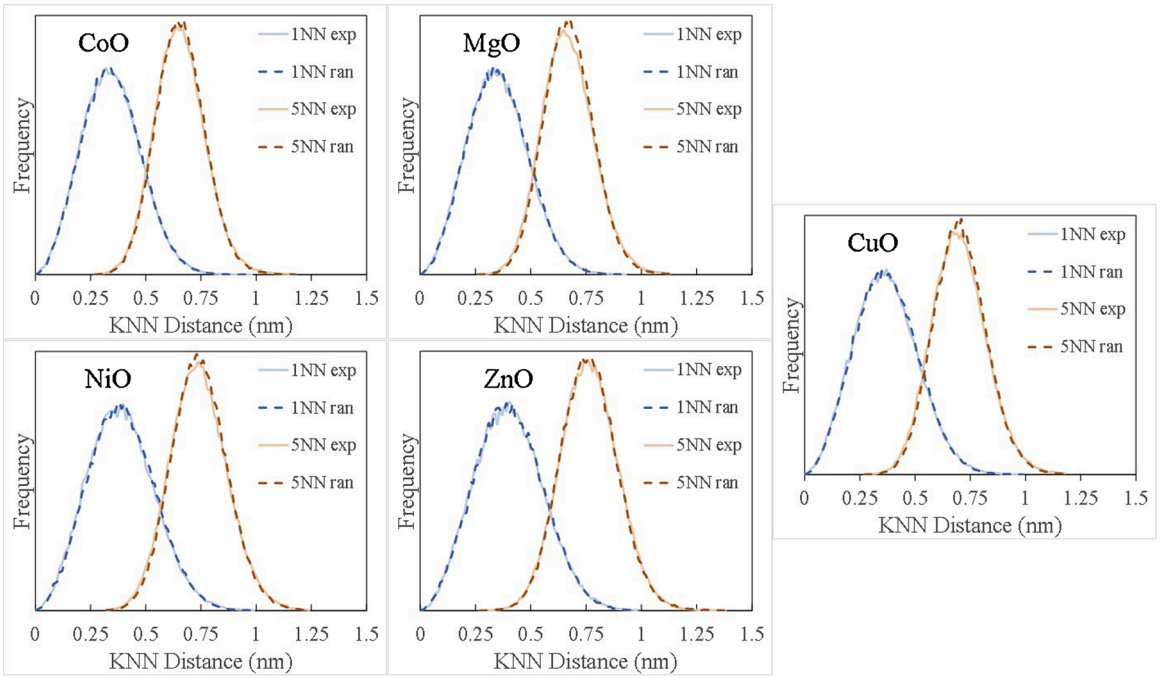

Fig. 7. Evaluation of chemical segregation in a single-phase coarse-grain sample: nearest neighbor (NN) analysis for a single-phase coarse-grain sample. Displayed are the distributions of the 1st nearest neighbor (1NN) and 5th nearest neighbor (5NN) distances for CoO, MgO, NiO, ZnO, and CuO. The measured distributions are compared to a randomized data set (dashed lines).

Table 1
Pearson coefficients calculated from the frequency distribution analysis for the single-phase coarse grain and single-phase nanocrystalline samples.

Sample	CoO	CuO	NiO	MgO	ZnO
Coarse	0.26	0.30	0.12	0.29	0.43
Nanocrystalline	0.17	0.22	0.14	0.16	0.16

processing times involved in SPS (5 min) allow thermodynamic and microstructural equilibrium to be avoided, restricting grain growth as well as significant formation of enthalpy-driven phases. The kinetics involved in the formation of the Cu-rich tenorite phase are slow enough that 5 min at 700 °C is not enough time for significant phase segregation.

It is important to remember that our single-phase coarse-grain samples were consolidated from blended oxide nanopowders using conventional sintering, while our single-phase nanocrystalline samples were consolidated from single-phase pre-reacted nanopowders using SPS. Despite being prepared using different powder synthesis and processing methods, both samples display a similar lack of significant inhomogeneity at the nm scale. The Pearson coefficients for both samples are much less than 1, indicating no significant chemical clustering. The low Pearson coefficients and lack of isolated binary oxide particles suggest that the solid-state reaction is complete in both single-phase samples. However, all of the Pearson coefficients measured in this study are greater than 0, indicating a non-random chemical distribution throughout the measured volume. We attribute this non-random distribution to local regions that are enriched in those elements [26]. The source of this local density fluctuation is likely related to the competition between entropy and enthalpy in TM-HEO. Our previous work found that enthalpy driven phase segregation occurred in TM-HEO at temperatures in the range of 650–850 °C [9]. Although, our single-phase coarse-grain samples are quenched, they will still spend a non-negligible amount of time at temperatures between 650 and 850 °C, allowing for small fluctuations in local chemistry to form. Similarly, our single-phase nanocrystalline samples are consolidated at 700 °C for 5 min, providing sufficient time for the formation of local variations in chemistry.

XRD, EDS, and APT all have different measurement volumes and resolution capabilities. When used together, the three techniques provide a powerful approach for studying phase homogeneity of HEO materials across a wide range of length scales. Using these three techniques,

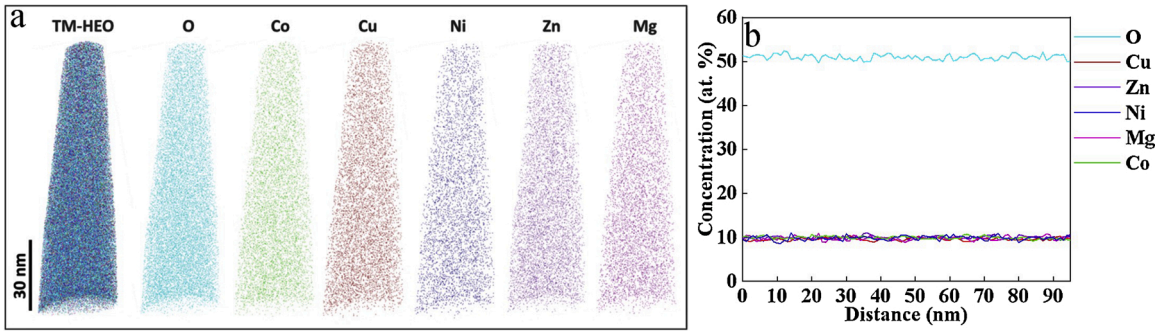

Fig. 8. Chemical distribution in a single-phase nanocrystalline sample: (a) atom probe tomography (APT) 3D chemical distribution maps for a sintered single-phase nanocrystalline sample; and (b) compositional profiles measured along a 6 nm diameter cylinder in a sintered single-phase nanocrystalline APT sample.

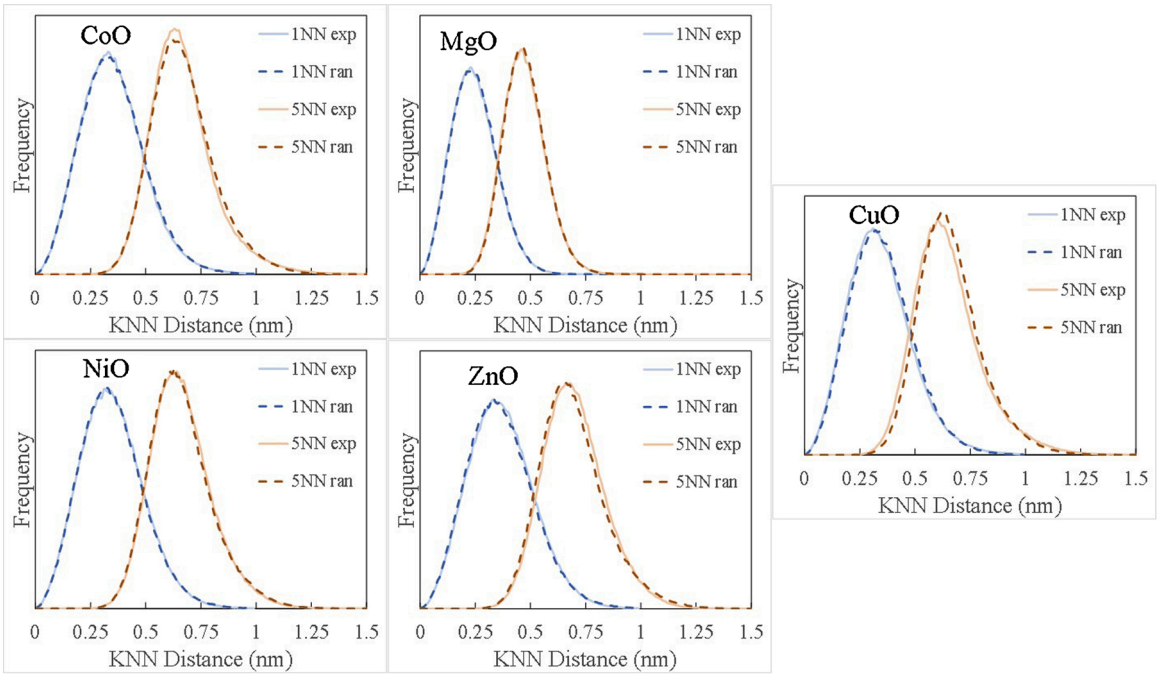

Fig. 9. Evaluation of chemical segregation in a single-phase nanocrystalline sample: nearest neighbor (NN) analysis for a single-phase nanocrystalline sample. Displayed are the distributions of the 1st nearest neighbor (1NN) and 5th nearest neighbor (5NN) distances for CoO, MgO, NiO, ZnO, and CuO. The measured distributions are compared to a randomized data set (dashed lines).

we have shown that our bulk single-phase TM-HEO samples have no significant chemical clustering or phase separation across multiple length scales, as illustrated schematically in Fig. 10. Note that the schematic is only meant to depict the chemical homogeneity in the sample and is not meant to imply any knowledge of the distribution of individual atoms. Critically, APT reveals that the solid-state reaction is complete down to the nm scale. The single-phase state can be achieved in both coarse-grain and nanocrystalline bulk TM-HEO after sintering and does not need to be sacrificed to produce a bulk sample with a desired grain size. Although phase homogeneity has been observed in

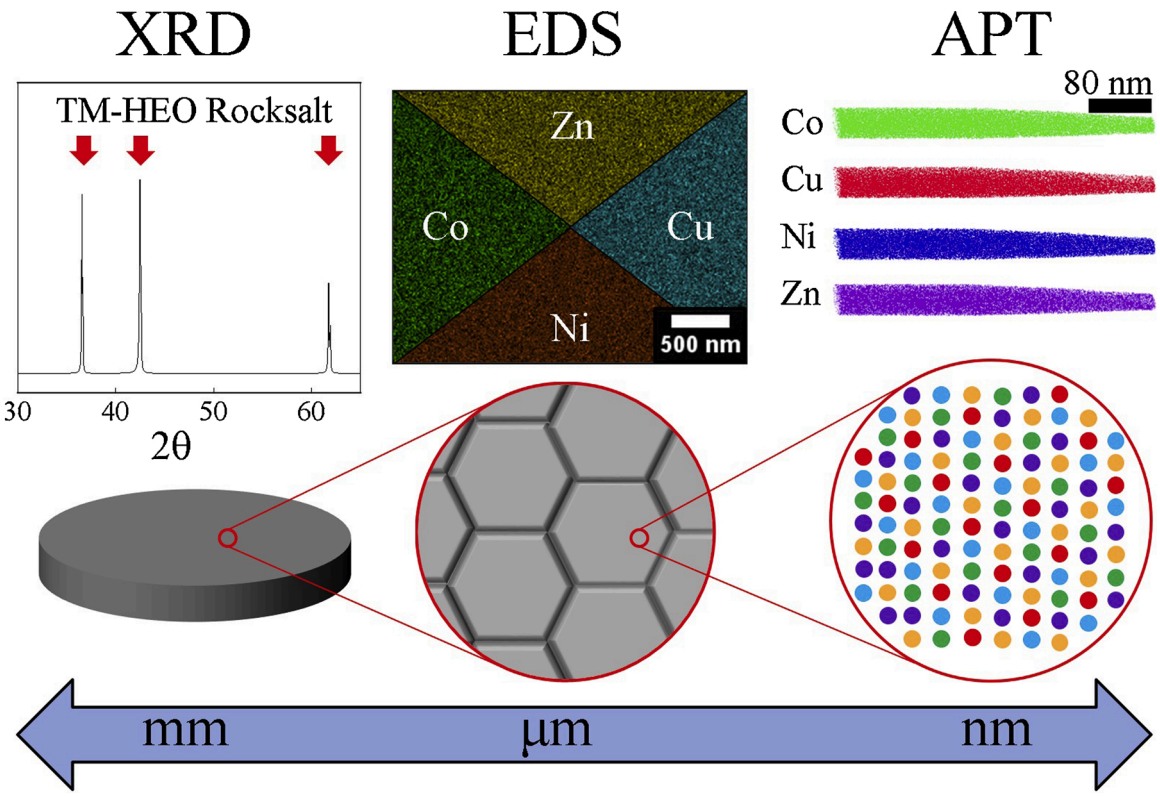

Fig. 10. Multiple length-scale phase homogeneity: Schematic illustrating that our sintered single-phase TM-HEO samples possess phase homogeneity across multiple length scales.

green bodies of nebulized spray pyrolysis powders [15], this is the first time that nm scale phase homogeneity has been observed using APT in sintered coarse-grain and nanocrystalline TM-HEO. It is important to note that, as a result of this study, phase homogeneity has now been observed in TM-HEO samples made with a wide range of powder synthesis and consolidation techniques. The entropy stabilized, single-phase state in HEOs is therefore more robust than would intuitively be expected, opening the door for bulk HEO materials to be utilized in a variety of solid-state applications without fear of compromising the phase stability.

4. Conclusions

Three types of TM-HEO samples were prepared using three different processing routes: single-phase coarse-grain samples prepared by reaction sintering unreacted nanopowders using conventional sintering at high temperatures, unreacted nanocrystalline samples prepared by consolidating unreacted nanopowders using spark plasma sintering (SPS) at low temperatures, and single-phase nanocrystalline samples prepared by consolidating solid-state pre-reacted nanopowders using SPS at low temperatures. XRD confirms that the single-phase coarse-grain and single-phase nanocrystalline samples possess a macroscopic single-phase rocksalt crystal structure, while the unreacted nanocrystalline samples possessed additional phases corresponding to the constituent oxide nanopowders. EDS indicates that the single-phase samples possess little-to-no secondary phase segregation, while the unreacted nanocrystalline samples possesses significant inhomogeneities that are similar in size to the constituent oxide nanopowders. APT measurements demonstrate that sintered single-phase samples lack significant chemical clustering at the nm scale. By combining all three measurement techniques, we observe that both single-phase coarse-grain and single-phase nanocrystalline TM-HEO samples possess phase homogeneity across multiple length scales. TM-HEO can be prepared using different processing methods while still achieving full phase homogeneity and a wide range of grain sizes. These findings suggest that the entropy stabilized single-phase states in HEO materials are stable enough to be processed using a variety of different techniques without endangering the desired multiscale phase homogeneity.

Declaration of Competing Interest

The authors report no declarations of interest.

Acknowledgements

SEM and XRD characterization was performed at the UC Irvine Materials Research Institute (IMRI). The authors are grateful to the Karlsruhe Nano Micro Facility (KNMF) for support and access to APT and FIB facilities. HH acknowledges financial support by Deutsche Forschungsgemeinschaft under grant HA1344/43-1. ADD and JMS acknowledge financial support from the UCI Samueli School of Engineering and the National Science Foundation under award CMMI-2029966 for experimental and analytical work, respectively. This work was also funded by the UC Irvine MRSEC, Center for Complex and Active Materials, under National Science Foundation award DMR-2011967.

References

[1] C.M. Rost, E. Sachet, T. Borman, A. Moballegh, E.C. Dickey, D. Hou, J.L. Jones, S. Curtarolo, J.-P. Maria, Entropy-stabilized oxides, Nat. Commun. 6 (2015) 8485, https://doi.org/10.1038/ncomms9485.

[2] D. Bérardan, S. Franger, D. Dragoe, A.K. Meena, N. Dragoe, Colossal dielectric constant in high entropy oxides, Phys. Status Solidi - Rapid Res. Lett. 10 (2016) 328–333, https://doi.org/10.1002/pssr.201600043.

[3] H. Chen, J. Fu, P. Zhang, H. Peng, C.W. Abney, K. Jie, X. Liu, M. Chi, S. Dai, Entropy-stabilized metal oxide solid solutions as CO oxidation catalysts with high-temperature stability, J. Mater. Chem. A 6 (2018) 11129–11133, https://doi.org/10.1039/C8TA01772G.

[4] D. Bérardan, S. Franger, A.K. Meena, N. Dragoe, Room temperature lithium superionic conductivity in high entropy oxides, J. Mater. Chem. A 4 (2016) 9536–9541, https://doi.org/10.1039/C6TA03249D.

[5] A. Sarkar, R. Djenadic, D. Wang, C. Hein, R. Kautenburger, O. Clemens, H. Hahn, Rare earth and transition metal based entropy stabilised perovskite type oxides, J. Eur. Ceram. Soc. 38 (2018) 2318–2327, https://doi.org/10.1016/j.jeurceramsoc.2017.12.058.

[6] K. Chen, X. Pei, L. Tang, H. Cheng, Z. Li, C. Li, X. Zhang, L. An, A five-component entropy-stabilized fluorite oxide, J. Eur. Ceram. Soc. 38 (2018) 4161–4164, https://doi.org/10.1016/j.jeurceramsoc.2018.04.063.

[7] A. Sarkar, L. Velasco, D. Wang, Q. Wang, G. Talasila, L. de Biasi, C. Kübel, T. Brezesinski, S.S. Bhattacharya, H. Hahn, B. Breitung, High entropy oxides for reversible energy storage, Nat. Commun. 9 (2018) 3400, https://doi.org/10.1038/s41467-018-05774-5.

[8] W. Hong, F. Chen, Q. Shen, Y. Han, W.G. Fahrenholtz, L. Zhang, Microstructural evolution and mechanical properties of (Mg,Co,Ni,Cu,Zn)O high-entropy ceramics, J. Am. Ceram. Soc. 102 (2019) 2228–2237, https://doi.org/10.1111/jace.16075.

[9] A.D. Dupuy, X. Wang, J.M. Schoenung, Entropic phase transformation in nanocrystalline high entropy oxides, Mater. Res. Lett. 7 (2019) 60–67, https://doi.org/10.1080/21663831.2018.1554605.

[10] M.R. Chellali, A. Sarkar, S.H. Nandam, S.S. Bhattacharya, B. Breitung, H. Hahn, L. Velasco, On the homogeneity of high entropy oxides: an investigation at the atomic scale, Scr. Mater. 166 (2019) 58–63, https://doi.org/10.1016/j.scriptamat.2019.02.039.

[11] D. Blavette, A. Bostel, J.M. Sarrau, B. Deconihout, A. Menand, An atom probe for three-dimensional tomography, Nature 363 (1993) 432–435, https://doi.org/10.1038/363432a0.

[12] A.D. Dupuy, Y. Kodera, G.P. Carman, J.E. Garay, Effect of phase homogeneity and grain size on ferroelectric properties of $0.5Ba(Zr_{0.2}Ti_{0.8})O_3$–$0.5(Ba_{0.7}Ca_{0.3})TiO_3$ (BXT) lead-free ceramics, Scr. Mater. 159 (2019) 13–17, https://doi.org/10.1016/j.scriptamat.2018.08.051.

[13] A. Sarkar, Q. Wang, A. Schiele, M.R. Chellali, S.S. Bhattacharya, D. Wang, T. Brezesinski, H. Hahn, L. Velasco, B. Breitung, High-entropy oxides: fundamental aspects and electrochemical properties, Adv. Mater. 31 (2019), 1806236, https://doi.org/10.1002/adma.201806236.

[14] C. Oses, C. Toher, S. Curtarolo, High-entropy ceramics, Nat. Rev. Mater. 5 (2020) 295–309, https://doi.org/10.1038/s41578-019-0170-8.

[15] A. Sarkar, R. Djenadic, N.J. Usharani, K.P. Sanghvi, V.S.K. Chakravadhanula, A. S. Gandhi, H. Hahn, S.S. Bhattacharya, Nanocrystalline multicomponent entropy stabilised transition metal oxides, J. Eur. Ceram. Soc. 37 (2017) 747–754, https://doi.org/10.1016/j.jeurceramsoc.2016.09.018.

[16] M.K. Miller, K.F. Russell, K. Thompson, R. Alvis, D.J. Larson, Review of atom probe FIB-based specimen preparation methods, Microsc. Microanal. 13 (2007) 428–436, https://doi.org/10.1017/S1431927607070845.

[17] M.J. Yao, K.G. Pradeep, C.C. Tasan, D. Raabe, A novel, single phase, non-equiatomic FeMnNiCoCr high-entropy alloy with exceptional phase stability and tensile ductility, Scr. Mater. 72–73 (2014) 5–8, https://doi.org/10.1016/j.scriptamat.2013.09.030.

[18] M.P. Moody, L.T. Stephenson, A.V. Ceguerra, S.P. Ringer, Quantitative binomial distribution analyses of nanoscale like-solute atom clustering and segregation in atom probe tomography data, Microsc. Res. Tech. 71 (2008) 542–550, https://doi.org/10.1002/jemt.20582.

[19] L. Lutterotti, M. Bortolotti, G. Ischia, I. Lonardelli, H.-R. Wenk, Rietveld texture analysis from diffraction images, Zeitschrift Für Krist 26 (2007) 125–130, https://doi.org/10.1524/zksu.2007.2007.suppl_26.125. Suppl.

[20] Z.F. Ma, G.C. Liang, J.S. Liang, Crystal defect behaviors in CeO2-based electrolyte doped with alkaline earth oxides, Acta Physico-Chim. Sin. 21 (2005) 663–667, https://doi.org/10.3866/PKU.WHXB20050617.

[21] M.Y. Yin, X.C. Wang, W.B. Mi, G.F. Chen, B.H. Yang, A first-principles prediction on the magnetism in CoO with Co and O Vacancies, J. Alloys Compd. 610 (2014) 422–427, https://doi.org/10.1016/j.jallcom.2014.05.040.

[22] W.B. Zhang, N. Yu, W.Y. Yu, B.Y. Tang, Stability and magnetism of vacancy in NiO: a GGA+U study, Eur. Phys. J. B 64 (2008) 153–158, https://doi.org/10.1140/epjb/e2008-00303-x.

[23] W.J. Tomlinson, A. Easterlow, Kinetics and microstructure of oxidation of CoO to Co3O4 at 700–800°C, J. Phys. Chem. Solids 46 (1985) 151–153, https://doi.org/10.1016/0022-3697(85)90211-2.

[24] K.M. Nam, J.H. Shim, D.-W. Han, H.S. Kwon, Y.-M. Kang, Y. Li, H. Song, W.S. Seo, J.T. Park, Syntheses and characterization of wurtzite CoO, rocksalt CoO, and spinel Co 3 O 4 nanocrystals: their interconversion and tuning of phase and morphology, Chem. Mater. 22 (2010) 4446–4454, https://doi.org/10.1021/cm101138h.

[25] D. Klissurski, E. Uzunova, Synthesis and features of binary cobaltite spinels, J. Mater. Sci. 29 (1994) 285–293, https://doi.org/10.1007/BF01162484.

[26] J. Hernández-Saz, M. Herrera, J. Pizarro, P.L. Galindo, M. Gonzalez, J. Abell, R. J. Walters, S.I. Molina, S. Duguay, Influence of the growth temperature on the composition distribution at sub-nm scale of InAlAsSb for solar cells, J. Alloys Compd. 763 (2018) 1005–1011, https://doi.org/10.1016/j.jallcom.2018.05.333.